Bangladesh J. Bot. **52**(2): 679-688, 2023 (June) Special DOI: https://doi.org/10.3329/bjb.v52i20.68321

A NEW APPROACH TO 3D DIGITAL EVALUATION AND ANALYSIS IN GEOLOGICAL ENGINEERING

JING GAO*[1], SHUWU LI, CHANGHU LI, ZHENGZHENG LI, XIAOFAN AN*[1], WENDONG FAN, YAN TONG, ZHU YANG AND TINGYU ZHANG[2]

Northwest Engineering Corporation Limited of PowerChina, No.18 East Zhangba Road, Yanta District, Xi'an, Shaanxi Province, 710065, China

Key words: Hydropower engineering, Geological digital cataloging, Three-dimensional geological analysis, DSI interpolation, Rock mass quality

Abstract

The initial geological analysis of hydropower projects is greatly complicated by the existence of complex geological conditions. To adapt advances in informatization and digitalization to the needs of the engineering survey industry and to conduct geological analysis more intuitively, in the present study the development of "GeoBIM", a geological 3D design platform based on the DSI modeling engine and a "graphics + data" architecture is rerported. GeoBIM realized the integration of 3D information in the whole process of geological work, from field data collection, model design, and analysis to approval. Taking the siting and construction of a hydropower station as an example, the field data collection and cataloging APP (boreholes, caverns, slopes) and web-side exploration monitoring platform of GeoBIM were used to build a 3D geological fine visualization model. The principle of dissipated energy was used to analyze the quality of the rock mass, which showed the spatial distribution characteristics of local geological conditions and rock mass quality, improving the efficiency and intuitiveness of engineering rock mass quality classification. GeoBIM was compared with traditional 2D geological analysis methods and actual conditions to demonstrate the rationale and intuitive use of the 3D digital evaluation method in geological engineering.

Introduction

Traditional three dimensional (3D) geological surveys mainly determine the deep information of the geological body manually through a comprehensive study of geological and section maps, measured field profiles, analysis of samples from boreholes, and other plane two dimensional **(**2D) and elevation 2D data, and expresses the distribution of surface geological bodies in 3D space a "pseudo 3D" form, or through a projection or overlay study on multiple planes, expressing comprehensive geological laws (Houlding 1994, Wu *et al.* 2003, Caumon *et al.* 2004, Cheng *et al.* 2004, Yang *et al.* 2015). True 3D geological modeling makes full use of data that can reflect deep information, such as geology, exploration, and testing, and computer graphics to realize a 3D visualization.

The main underlying technology used in geological 3D research and development is Kriging interpolation (Mallet 2002). Platforms vary, but the kernels are all Kriging interpolation or improved Kriging interpolation. However, this algorithm can only be used to construct some relatively simple nonlinear geological interfaces, and there are many problems such as information loss, model distortion, and invalid geological evaluation (Li 1994, Caumon and Mallet 2003, Tan 2005, Han and Zhu 2006, Yang *et al.* 2007, Chai 2016) and they are all based on modeling, and

*Author for correspondence: <zjdyggj@163.com>. [1]High Slope and Geological Hazard Research & Management Branch, National Energy and Hydropower Engineering Technology R&D Centre, 710065 Xi'an, Shaanxi, China. [2]Shaanxi Local Construction Land Engineering Technology Research Institute Co., Ltd, 710082 Xi'an, Shaanxi, China.

the model is less used in analysis and calculation (Wang *et al.* 2003, Caumon *et al.* 2004, Sprague and Kemp 2005, Kaufmann and Martin 2007). In the modeling process, the construction of the geometric shape of the geological body and the construction of the binary structure of the geological body attributes (such as the Rock Quality Designation (RQD) value and the Lugeon value) revealed by the exploration and geophysical prospecting, must also be taken into account, as the final constructed geological body is used for analysis and application, such as 2D geological mapping, and rock mass quality classification (Wang *et al.* 2012). Given the characteristics and requirements of 3D geological modeling, it is proposed in the present study that more suitable methods should be used for modeling and geological analysis in practice. One such method is Discrete Smooth Interpolation (DSI) technology (Briggs 1974). Compared with traditional modeling algorithms, the advantage of DSI technology is that it can fit and construct complex (i.e., folds and lenses), discontinuous (i.e., faults and overburden) geological structures with binary structures in real-time according to various constraints. Although the geological modeling capability of GoCAD based on DSI technology is very prominent, this product is mainly tailored to the needs of the petroleum industry (Mallet 1992, Zhang *et al.* 2015).

The present study used Geology-Building Information Modeling (GeoBIM), a geological 3D modeling platform developed with the latest 3D geological modeling ideas, as the object and combines engineering examples and modeling ideas to create a 3D geological model and conduct geological model analysis and application research. Learning from the successful experience of other geological 3D software and summarizing the lessons of failure, GeoBIM chose modeling based on DSI as its underlying technology and solved the adaptability problem of the hydropower industry through secondary development (Xiong *et al.* 2007, Po-Tsun 2020, Chen 2021). This method is especially suitable for 3D modeling of discontinuous, nonlinear and binary geological bodies. It can provide more abundant and intuitive geological analysis data for the information design of similar projects, and is conducive to observing and analyzing the geological state of the engineering area.

Materials and Methods

First, a 3D geological discrete model $M(\Omega, N, \varphi, C)$ was defined, where Ω is all nodes that make up the model, N is the field point set of each node, φ is the nth order vector property function of each node, and C is the constraint of each node.

Then the global roughness function was defined as:

$$R^*(\phi) = R(\phi) + \emptyset * \overline{\omega} * \rho(\phi)$$

where $R(\phi)$ is the global roughness function, $\rho(\phi)$ is the global constraint violation function, $\emptyset$ is the constraint factor, and $\overline{\omega}$ is the balance factor.

The DSI solution is found by minimizing the function $R^*(\phi)$, which is when $\frac{\partial R^*(\phi)}{\partial \phi} = 0$. Therefore:

$$\phi^v(\alpha) = -\frac{G^v(\alpha \mid \phi) + (\emptyset.\overline{\omega}).\Gamma^v(\alpha \mid \phi)}{g^v(\alpha) + (\emptyset.\overline{\omega}).\gamma^v(\alpha)} \qquad (1)$$

where :

$$G^v(\alpha \mid \phi) = \sum_{k \in N(\alpha)} \{\mu(k).v^v(k,\alpha).\sum_{\substack{\alpha \in N(k) \\ \beta \neq \alpha}} v^v(k,\beta).\varphi^v(\beta)$$

$$g^v(\alpha) = \sum_{k \in N(\alpha)} \mu(k).(v^v(k,\alpha))^2$$

$$\Gamma^{v}(\alpha|\varphi) = \sum_{c\in C^{\simeq}} \bar{\omega}_c . \Gamma_c^{v}(\alpha|\varphi)$$

$$\gamma^{v}(\alpha) = (A_c^{v}(\alpha))^2$$

$$\Gamma_c^{v}(\alpha|\varphi) = A_c^{v}(\alpha).\{\sum_{\beta\neq\alpha} A_c^{v}(\beta).\varphi^{v}(\beta) - b_c + x_c^{v}(\alpha|\varphi)\}$$

$$x_c^{v}(\alpha|\varphi) = \sum_{\eta\neq v}\sum_{\beta} A_c^{\eta}(\beta).\varphi^{\eta}(\beta)$$

$A_c^{v}(\alpha)$ is the constraint coefficient, and, according to the actual constraints, the constraint coefficients under different conditions can be obtained, which allows the optimal φ value to be iteratively solved by Equation (1). The actual constraints include the interface position, occurrence, fault throw, and dislocation direction revealed by drilling. These can be regarded as either hard constraints or soft constraints, with hard constraints referring to those that must be fitted 100% accurately, such as the position of the layers revealed by drilling holes, while soft constraints, such as fault dislocation direction and estimated fault throw, can be fitted with weighting factors according to the reliability of specific exploration or geophysical exploration.

GeoBIM 3D geological modeling software is based on the object-oriented classification approach. Based on the resulting 3D unified model, a series of geological analysis applications, including rock mass quality visualization classification, 3D model arbitrary section analysis, and dam and underground engineering geological analysis, can be used to provide a theoretical basis for analyzing geological problems in the survey, design, and construction of water conservancy and hydropower projects under complex geological conditions and technical means.

Results and Discussion

First, a database was built consisting of all exploration results from the available sources of project data, which not only facilitates the preservation and management of data but also provides a basis for subsequent analysis and application models (Fig. 1).

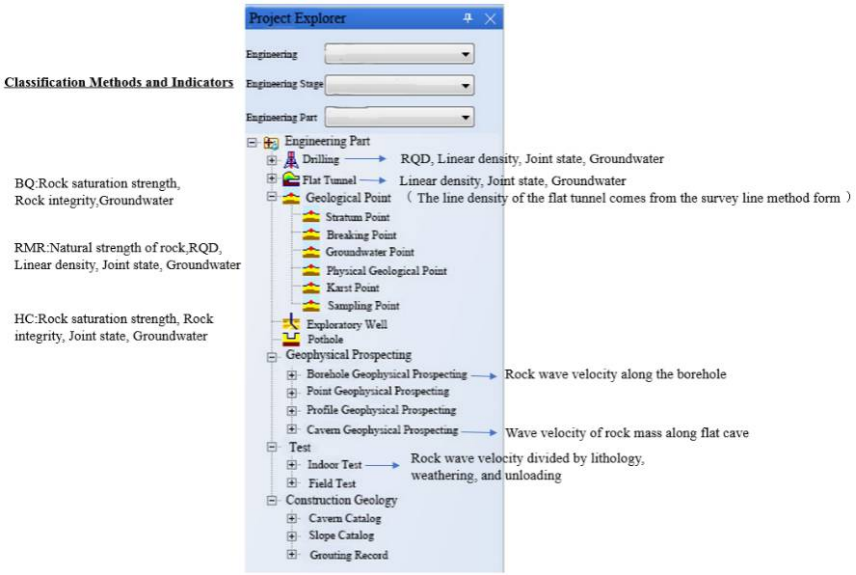

Fig. 1. The indexes required for the grading and database entry methods.

Exporting the database to the 3D display interface allows the RQD of the survey layout and survey results to be easily viewed (Fig. 2).

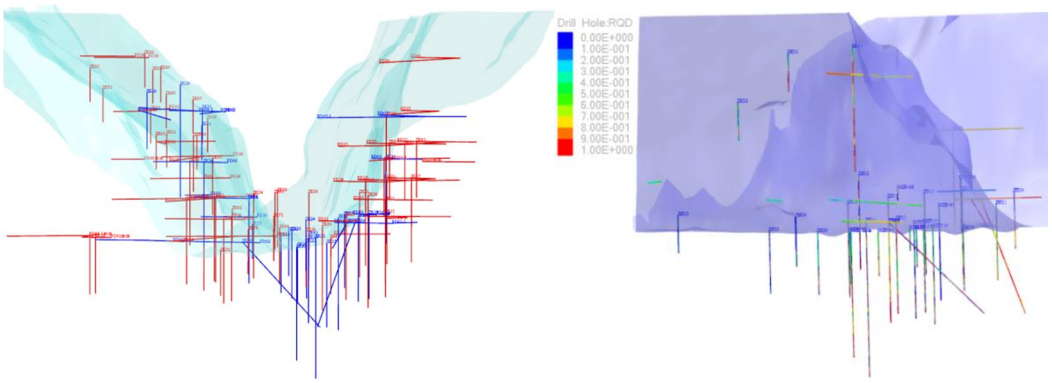

Fig. 2. 3D display of the exploration point layout.

From the single-index spatial achievement data formed in the database (point cloud + attribute format, imported to the 3D visualization platform through the import point set command) combined with the magnetotelluric method for detection, it can be concluded that the depth of the cover layer is 30 m ~ 75 m. While the rock roof elevation changes in the range of 2950 to 3000 m (Fig. 3).

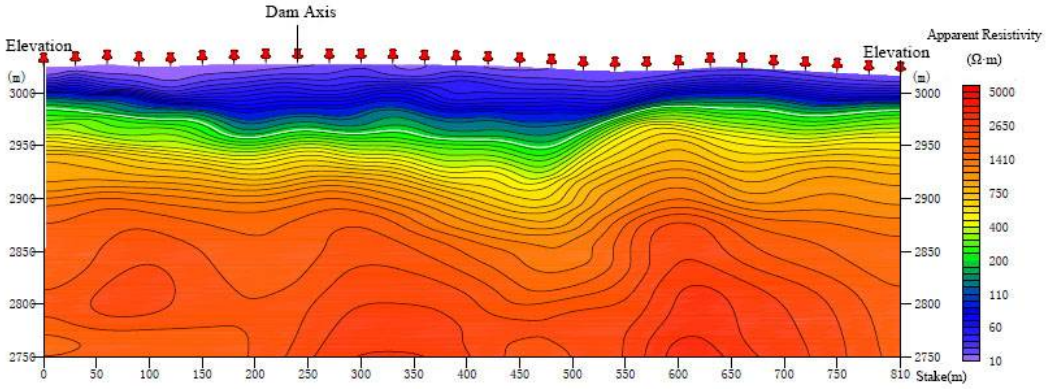

Fig. 3. A sectional view of representative survey line geophysical exploration results.

Data used for defining the topographic surface can be topographic point data, DEM data, elevation points, or contour lines. Figure 4 showed the 3D display of the topographic surface.

The 3D geological model is an underground 3D stratigraphic space based on the results of field exploration, such as geological exploration, geophysical exploration, surveying and mapping, and testing (Fig. 5). The boundary of each layer was determined through geological exploration, then the grid surface of each layer was created and defined. The geological attribute points formed by each exploration result were used to constrain the grid surface, and finally, a stratigraphic entity with geological attributes was formed. The size of the grid was controlled by the precision and density of the survey results.

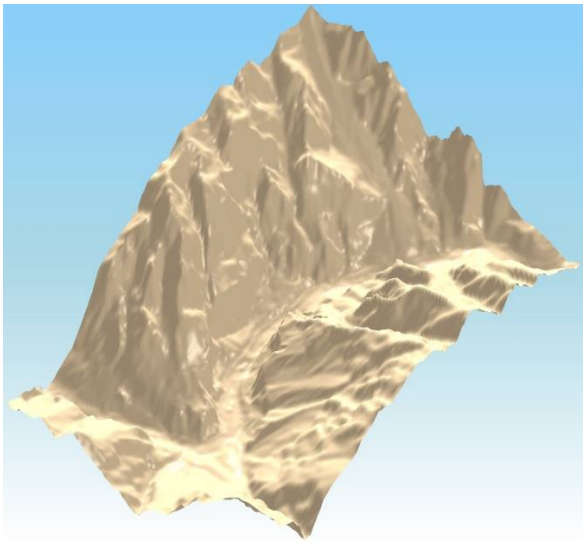

Fig. 4. 3D topographic map of the study area.

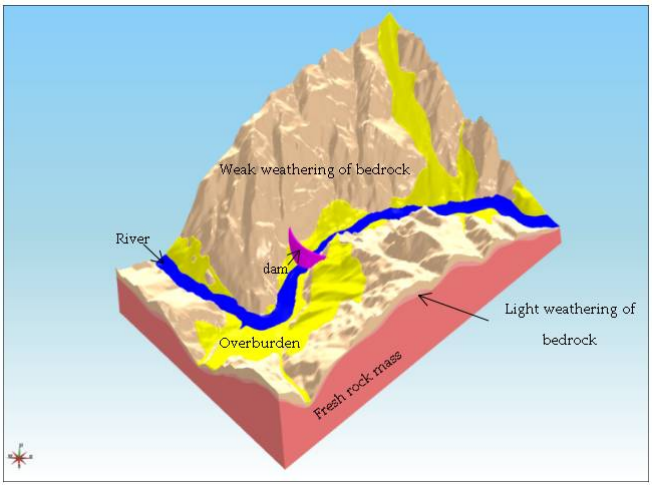

Fig. 5. 3D model of the engineering geology in the study area.

The 3D model of the structural surface of the study area was obtained from the exposed line and the occurrence of the structural surface (Fig. 6). Results showed that the faults in the engineering area are not well developed, and there are no long and weak structural planes that directly combine to form structural blocks on the left bank. The right bank was cut by small gullies downstream, and combined with some NNW-oriented structural planes and gently dipping structural planes; there are uncertain structural blocks. The right bank developed a combination of a gently dipping downstream structural plane, a near-EW-trending steeply dipping structural plane, and an NNW-trending steeply dipping structural plane. There was also an anti-slip stable block. The sideslip plane is a long and weak structural plane, and the anti-slip stability conditions of the right bank were worse than those of the left bank.

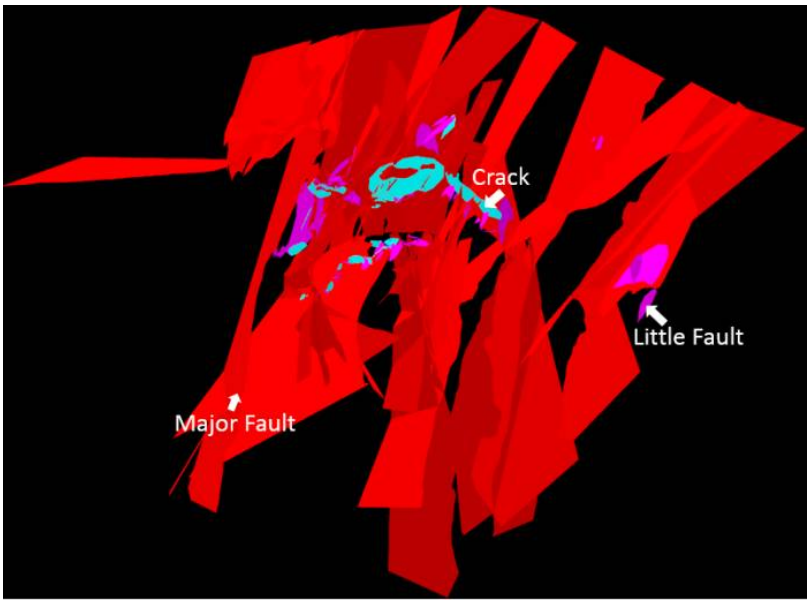

Fig. 6. 3D display of the structural plane distribution in the engineering area (Vertical view).

The RQD 3D isosurface map of the rock mass (Fig. 7) showed that with increasing tunnel depth, the degree of weathering and unloading of the rock mass gradually weakens. When RQD > 80, the rock mass is considered to be of good quality. However, the quality of the rock mass was poor in the sections near the broken rock mass and unloading cracks and faults. On the same slope, the horizontal depth of the rock mass with poor quality in the flat cave increased with increasing elevation and was also more fragmented. The 3D display showed that the proportion of RQD types III_1~II in the engineering area was relatively high.

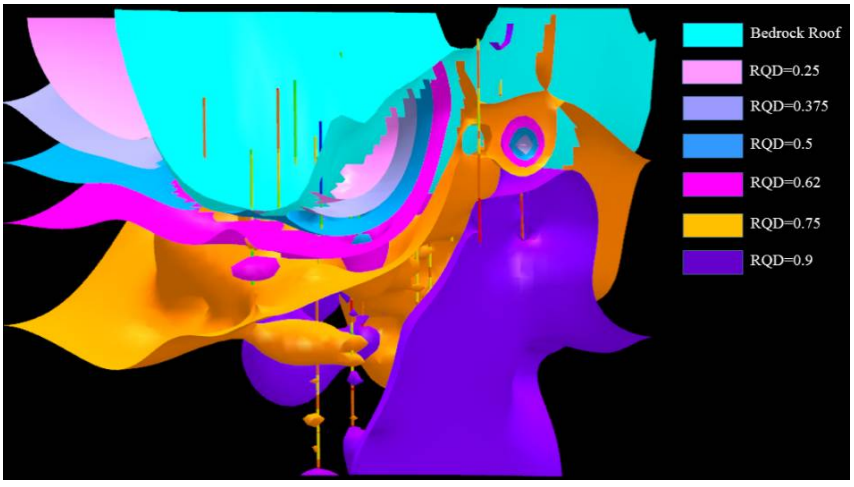

Fig. 7. RQD 3D isosurface map of the rock mass.

The 3D display of the rock mass wave velocity (Fig. 8) showed that the variation range of the longitudinal wave velocity, Vp, of the rock mass in each cave measured on the left bank of the lower dam site was 3550 – 5200 m/s, and the average value was 4580 m/s. There are more rock masses with 4450 < Vp ≤ 5200m/s and Vp > 5200m/s, accounting for 33.3 and 45.2% of the measured rock masses, respectively, while the proportion of rock masses with Vp ≤ 4450m/s is relatively small, of which only 2.4% is broken rock mass, with no broken rock mass. The spatial distribution of the low-velocity parts shows that the relatively broken rock mass is in the shallow part of the mountain in the range of 0 – 35m. This showed that the fissures and structural planes in the middle-deep rock mass are relatively undeveloped and that the rock mass quality is generally good.

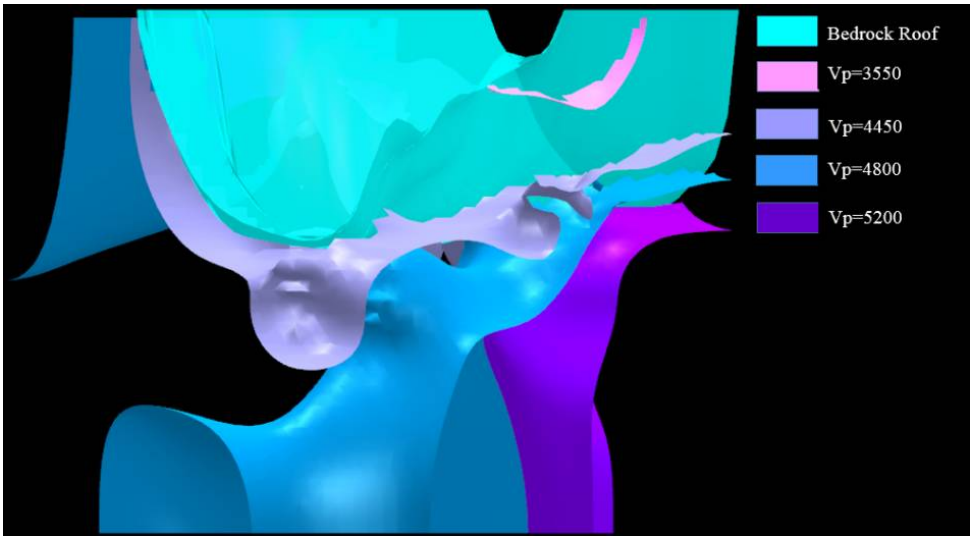

Fig. 8. 3D isosurface map of the rock mass wave velocity.

The 3D analysis for the rock mass quality classification implements the method of “single index scoring and summation”, that is, data of every single index are collected on-site, and then the rock mass quality is obtained by summing. The rock mass quality classification of 3D methods of RMR, hydropower, and BQ function is provided by the software. All three grading methods are the summation of single index values. The single indices required for the accumulation of the 3D methods include rock uniaxial compressive strength UCS (RMR uses natural sample index, the rest uses saturation value), joint surface state, groundwater condition, RQD and joint spacing (RMR), and rock mass wave velocity (hydro and BQ). Once these single index values are collected and stored in the database, the basic data on which the rock mass quality classification depends are available. After the database index and structure-face-interpolated calculation of the rock layer, the rock mass classification starts. The program automatically sums up the classification of single indices in all cubic mesh grid cells within the classification range to complete the rock mass quality classification. After the classification is completed, the rock mass quality classification results at any point can be viewed by shifting the data plane in the XYZ direction. The rock mass quality at any point can also be obtained quantitatively by extracting the isosurface map of the rock mass quality classification index RMR (Fig. 9).

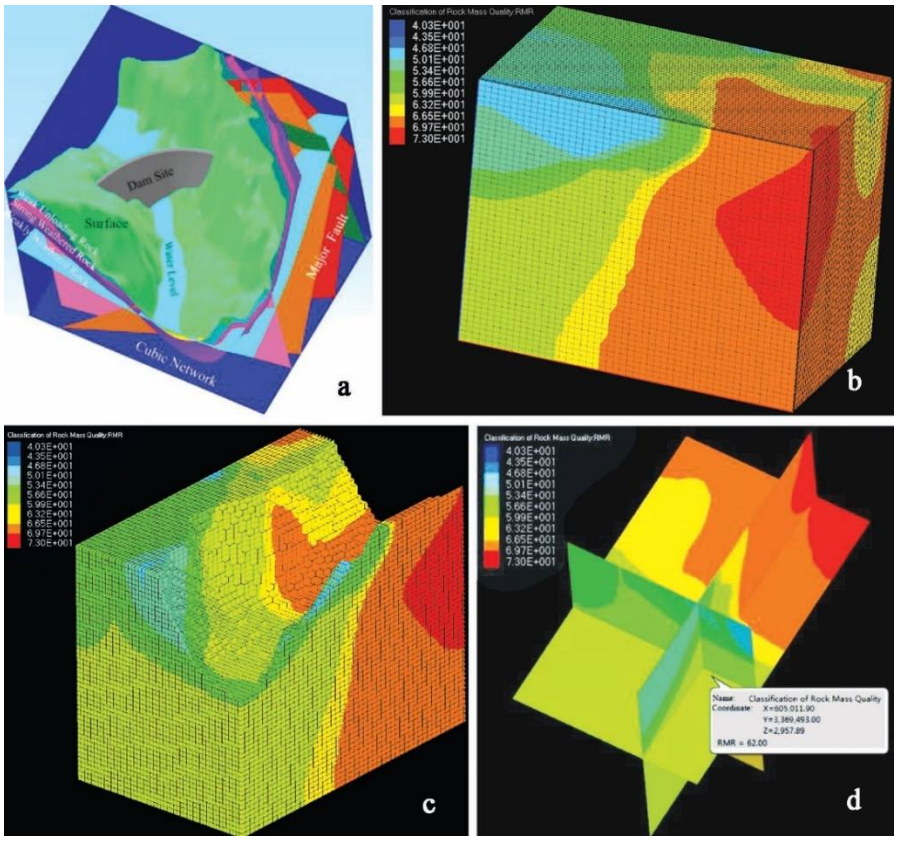

Fig. 9. Diagram of the rock mass quality classification process display.(a). The structural planes, rock planes and classification scope that need to be considered in classification; (b). The classification results of cubic network; (c). The overall effect of classification results; (d). The classification results of a certain position.

Finally, the classification results and parameter values can be displayed on the building profile surface, and the relevant parameter values of the cubic net can be "assigned" to the building profile (surface object) through the surface command to obtain the rock mass quality classification distribution map (Fig. 10).

To verify the practicability of this quality classification method, taking the above test area as an example, five representative measuring points in the flat tunnel of the lower dam site were selected to calculate their membership degrees at all levels, which were analyzed and then compared with the equivalent data obtained using a traditional comprehensive fuzzy discrimination method. The comprehensive rock quality index (P1), RQD index (P2), joint linear density index (P3), joint surface state index (P4), groundwater condition (P5), and other indicators were used to divide the rock mass quality into five categories. The measured values of the rock mass quality indicators of each sample are shown in Table 1 alongside the results of the on-site engineering geological survey and laboratory tests. Results showed that the prosed approach we are proposing returns almost identical results to the fuzzy comprehensive evaluation method and has a higher consistency with the on-site excavation results, which meets the engineering needs.

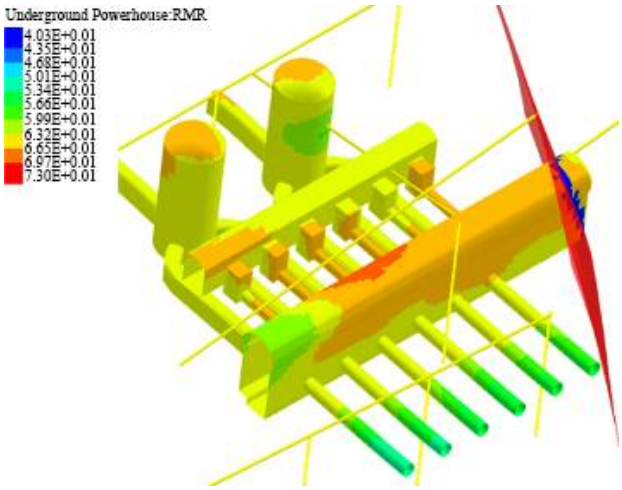

Fig. 10. A building outline provided by the rock mass quality classification results.

Table 1. Comparative analysis of the rock mass quality index classification results.

Sample	Evaluation indicators					Geo-BIM 3D method	Traditional 2D analysis method	On-site exposure
	P1	P2	P3	P4	P5			
1	45	30	0.18	0.49	15	III	III	III
2	51	47.6	0.44	0.48	9.8	III	II	III
3	30	38	0.34	0.33	16.3	IV	IV	IV
4	55	88	0.28	0.45	19	III	III	II~III
5	52	70.1	0.51	0.36	0.05	II	II	II

Unlike with traditional 2D engineering geological condition analysis, with the 3D geological model, the values of relevant parameters on all exploration points can be imported through the database in the GeoBIM software and assigned to the 3D geological model of the dam site area. The geological parameters of the rock mass can then be automatically obtained through interpolation, and the rock quality index RQD value, saturated uniaxial compressive strength value, water permeability Lv value, and other geological parameters can be visually checked through the 3D geological model. Users can generate the iosurface of a certain index, such as the isosurface of the rock quality index RQD = 80%, and judge the area with the rock quality index RQD > 80% in the rock layer through the isosurface.

A novel 3D geological modeling and analysis software was developed in the present study and a geological analysis was carried out of the siting and construction of a hydropower station based on the whole process of field data collection, exploration, modeling, and rock mass quality analysis. A comparison of the 3D analysis results of the whole process with the traditional 2D rock mass quality analysis and on-site exposed rock mass quality results demonstrates that the 3D analysis results are consistent with the actual situation and can therefore meet the engineering needs.

Acknowledgments

This research was supported by Natural Science Basic Research Program of Shaanxi (Program No.2022JQ-457).

References

Briggs IC 1974. Machine contouring using minimal curvature. Geophy. **39**(01): 39-48.

Caumon G and Mallet JL 2003. Interactive editing of sealed geological 3D Model. Int. Assoc. Mathem. Geol. **14**(2): 703-712.

Caumon G, François L and Sword CH 2004. Building and editing a sealed geological model. Mathem. Geol. **36**(4) : 405-424.

Cheng PG, Gong JY and Shi WZ 2004. Research on 3D modeling and application of geological body based on triangular prism. J. Wuhan Univer. Inform. Sci. Edition **29**(7): 602-307.

Chai Y 2016. Deep geological structure and three-dimensional geological model of the Liao-Ji rift in Dandong area. Jilin University, Jinlin. 38pp.

Chen CH 2021. Rapid identification of joints and fractures and 3D characterization of rock mass quality. Hefei University of Technology, Hefei. 52pp.

Han LT and Zhu Q 2006. An object-oriented 3d underground space vector data model. J. Jilin University, **36**(4):636-641.

Houlding SW 1994. 3D geoscience modeling: Computer techniques for geological characterization. Berlin: Spring-Verlag **31**(1): 135-137.

Kaufmann O and Martin T 2007. 3D geological modelling from boreholes, cross-sections and geological maps, application over former natural gas storages in coal mines. Comput. Geosci. **34**(3): 547-555.

Li R 1994. Data structures and application issues in 3D geographic information systems. GEOMATICA, **48**(W1):119-126.

Mallet JL 1992. Discrete smooth interpolation in geometric modeling. Computer-Aided Design **24**(4): 177-191.

Mallet JL 2002. Geomodeling. Oxford University Press, New York.121-122pp.

Po-Tsun Y, Kevin ZL and Kuang TC 2020. 3D Effects of permeability and strength anisotropy on the stability of weakly cemented rock slopes subjected to rainfall infiltration. Engin. Geol. **6**: 266.

Sprague KB and Kemp EAD 2005. Interpretive tools for 3D structural geological modelling part II: surface design from sparse spatial data. Geo Informatica **9**(1): 5-32.

Tan RC 2005. Integration and application of 3D spatial data model in GIS. Surveying Engin. **14**(1):63-66.

Wang CY, Bai SW and He HJ 2003. Research on geological modeling in 3d stratigraphic visualization. Chin. J. Rock Mechan. Engin. **22**(10): 1722-1722.

Wang XB, Li H and Zhang CF 2012. Application of DSI technology in 3D modeling of engineering geology. Proc. 2nd Engin. Geol. Symp. 5th Geol. Explor. Profess. Com., Wuhan.172pp.

Wu LX, Chen XX and Shi WZ 2003. True 3D spatial modeling of underground engineering and surrounding rock integration based on GTP. Geograp. Geograph. Inform. Sci. **6**: 5-10.

Xiong ZQ, He HJ and Xia YH 2007. Research on 3D stratigraphic modeling and visualization technology based on TIN. Geomech. **9**:190-194.

Yang WH, Yin L and Sun JY 2015. 3D stratigraphic modeling and visualization of mine drilling data. Metal Mine, **44**(10):130-134.

Yang DL, Zhang YB and Wang XC 2007. 3D modeling method and technical guide of geological body. Geological Press. 276pp.

Zhang CF, Zhou XJ and Jia XH 2015. Research and application of 3D visualization of geological information in hydropower engineering. Resour. Environ. Engin. **05**: 126-130.

Manuscript received on 03 March, 2023; revised on 10 August, 2023)